

Normal/shear cracking of brickwork masonry

E. Reyes, M.J. Casati & J.C. Gálvez

E.T.S. Ingenieros de Caminos, Universidad Castilla La Mancha, Ciudad Real, Spain.

ABSTRACT: The study of the brickwork masonry has been focused on the compression and compression/shear failure, and minor effort has been devoted to studying the tensile/shear failure (mixed mode I/II fracture). This paper shows a series of brickwork masonry tests under mixed mode loading. The tests were performed with two testing geometries: the three point bending test with a non-symmetric notch, and the double-edge notched specimen. The specimens were 1/4 scaled model of an ordinary single leaf brickwork masonry. To study the influence of the angle between of the cracks and the bed joints, different orientations of the bed joints were tested. Two similar sizes were tested to take into account the size effect. A numerical model for the mixed mode fracture of masonry is also presented. The model takes into account the anisotropy of the material and properly fits the experimental results.

Keywords: masonry, mixed mode, experimental, numerical modeling, cohesive models, anisotropy.

1 INTRODUCTION

Brickwork masonry structural elements and walls are very common in Europe, and specially in the Mediterranean countries. The brickwork masonry design codes are under the auspices of the concrete associations in many countries, this is the case of the ACI (1999a, b) in the USA. There are many reasons to justify this fact, but one of them, a technical reason, is that there are many common problems between concrete and brickwork masonry structural elements. One of them is the cracking problem of the walls, associated with the differential settlements and/or excessive deflections of the concrete slabs along the life of the structure. This problem is a fracture problem, where the wall is cracked under mixed mode fracture: tensile and shear stresses combination. This reason aimed us to present a paper about masonry fracture in a fracture of concrete structures conference: the brick masonry is a part, in many cases, of the concrete structure, and it is affected by the same fracture problems.

Brickwork masonry may be considered a composite material: mortar and bricks; and its mechanical properties, specially fracture properties,

depend on the properties of the components. The geometric disposition of the bricks in layers, bed joints, with inserted mortar, as well as, the interface between them, causes anisotropy on the mechanical behaviour and strength of the brickwork masonry.

Traditionally, the study of the brickwork masonry has been focussed on the compression and compression/shear failure mechanisms (Lorenço, 1996, Lorenço et al., 1996, Bosiljkov et al., 1998, Jukes & Riddintong, 2001), and minor effort has been devoted to studying the tensile/shear failure (mixed mode fracture). There are not enough experimental data for a good knowledge of the mixed mode fracture of the brickwork masonry, and to validate the mixed mode fracture models. This paper shows a complete series of brickwork masonry tests under mixed mode loading. The tests were performed with two testing geometries: the three point bending test with non-symmetric notch, and the double-edge notched specimen. Both testing procedures were successfully used by the authors for the mixed mode fracture of concrete (Gálvez et al., 1999, 2002a).

The brickwork masonry specimens were 1/4 scaled model of an ordinary single leaf brick masonry. To study the influence of the angle between



Figure 1. Testing arrangement to measure the fracture properties of the brick masonry (bed joints at 45°).

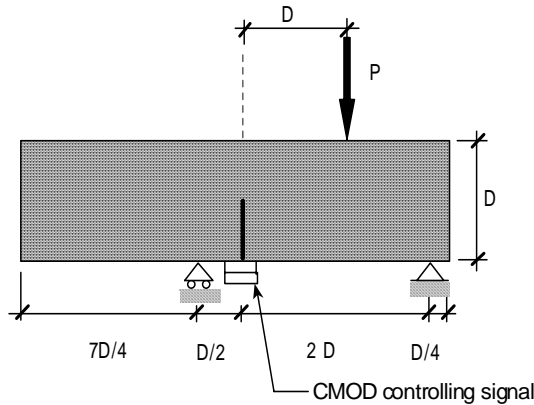


Figure 2. Testing arrangement, geometry and dimensions of the TPB specimens.

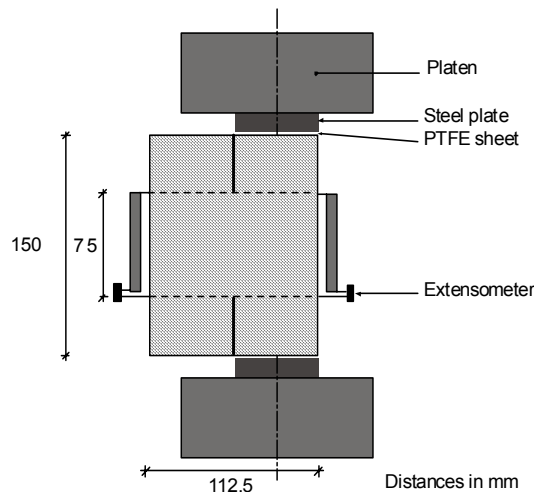


Figure 3. Testing arrangement, geometry and dimensions of the double-edge notched specimens.

of the crack and the bed joints, different orientations of the bed joints, respect to the notch plane, were tested: 0, 30, 45, 60, 90, -30, -45 and -60 degrees. Two homothetic sizes were tested to take into account the size effect.

A numerical model for the mixed mode fracture of the masonry is also presented. The model is an extension of the cohesive model developed by the authors (Gálvez et al., 2002a) for concrete, and take into account the anisotropy of the material. The model properly fits the experimental results.

2 EXPERIMENTAL PROGRAM

2.1 Materials and specimens

A 1/4 scale model of an ordinary single leaf brick masonry was used to make the specimens. The bricks were cut from solid clay commercial bricks, machined with a low speed diamond cutting disc. The dimensions of the resultant bricks were 48 x 24 x 10 mm. A single mortar mixture was used to cast the specimens. The mortar was composed of Portland cement and siliceous sand of 1 mm maximum size. The fracture energy of the brick, mortar and interface brick-mortar was measured: 107 N/m (brick), 86 N/m (mortar) and 10 N/m (interface). The tensile strength of the mortar was 7.5 N/mm², and 7.6 N/mm² for the brick.

The cut bricks for the specimens were immersed in lime saturated water at 20°C for 24 hours. Then, the specimens were cast horizontally in ground steel moulds. The bricks were fixed in the mould and the fresh mortar was poured over the matrix of bricks. Prismatic specimens of 150 x 675 x 26.2 mm were made, with three orientations of the joints: 0, 45 and 90 degrees. The thickness of the mortar joint was 3.0 mm.

To obtain the fracture mechanical properties of the brick masonry, the prisms were tested in accordance with RILEM 50-FMC (1986). Table 1 shows the mechanical properties of the masonry. Figure 1 shows the testing arrangement to measure the mechanical properties of the masonry under fracture.

For the TPB with a non-symmetric notch (see Fig.2) specimens of two similar sizes were cast. Table 2 shows the dimensions of the TPB specimens. Specimens with different angles between the notch and the bed joint were made: 0, 45, 90 and -45 degrees for both sizes. Specimens with 30, -30, 60 and -60 degrees were also tested with the small size of specimen.

Table 1. Mechanical properties of the brick masonry.

Orientation	G_F (N/m)	f_t (N/mm ²)	E (kN/mm ²)
horizontal	75	5.8	28
45°	54	4.1	22
vertical	33*	2.4*	21*

* Estimated

Table 2. Dimensions of the TPB specimens with non-symmetric notch (in mm).

Size	Depth D	Notch $D/2$	Length $4,5D$
large	150	75	675
small	75	37,5	337,5

Thickness: 26,5 mm

For the double-edge notched geometry, specimens with three different inclination of the bed joint were made: 0, 45 and 90 degrees. Figure 3 shows the geometry and dimensions of the specimens.

2.2 Experimental procedure

Figure 2 shows the experimental arrangement of the Three Point Bending (TPB) specimens with a non-symmetric notch. The tests were performed in CMOD control, at a rate of 0.04 mm/min until 80% of the peak load in the descending branch and 0.08 mm/min until the end of the test. Figure 4 shows a small specimen during testing. During the tests the following parameters were recorded: CMOD, load P and load point displacement of force P .

Figure 3 shows the testing arrangement of the double-notched specimens of the brick masonry under compression loading. Two ground and smooth steel plates were placed between the machine platens and the upper and bottom faces of the specimen to apply the compression load. To eliminate the friction between the steel plate and the concrete a Polytetrafluoro-ethylen (PTFE) sheet was inserted, the thickness of the PTFE sheet being 0.2 mm. Between the upper platen and the load cell there was a hinge. Initially a small compression load was applied over the specimen with free rotation hinge; then the hinge was fixed and the whole test was developed with the hinge fixed; in this way it is guaranteed that the compression load is uniformly applied over the whole surface of the steel plates. During the tests the following parameters were recorded: load P , displacement of the actuator and the relative displacement of the points situated at the height of the tip notches on the lateral vertical faces of the loaded and unloaded parts of the specimen, see Figure 3 for details.

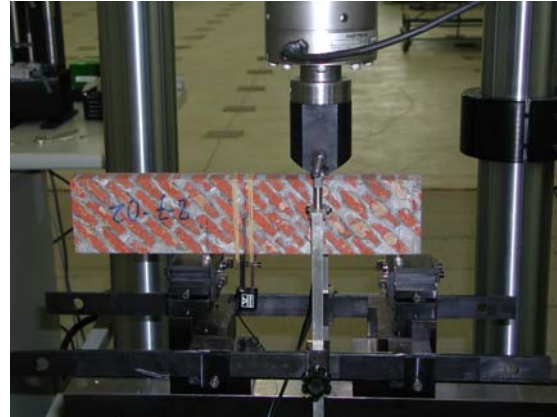


Figure 4. TPB small specimen ($D = 75$ mm), with the bed joints inclined -45° , during testing.

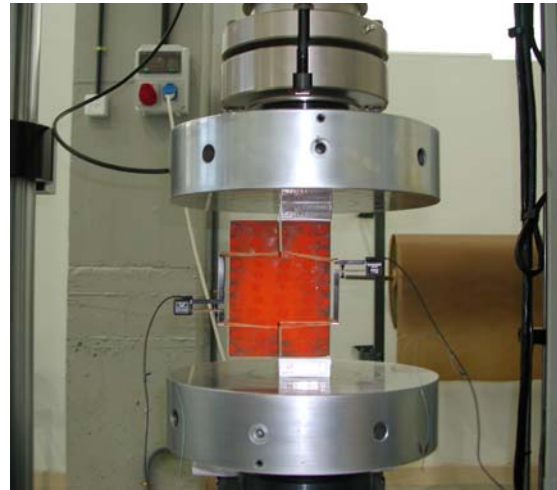


Figure 5. Double-edge notched specimen with the bed joints at 0° during testing.

The tests were performed in actuator displacement control, at a rate of 0.04 mm/min.

2.3 Testing equipment

The load P was applied by a servocontrolled closed-loop testing machine. The load P was measured with 5, 25 and 100 kN load cells with ± 0.1 percent error of cell-rated output. Extensometers, with ± 2.5 mm travel and ± 0.2 percent error at full scale displacement, were used to measure the relative displacement of the points in the double-edge notched specimens, and CMOD in the TPB specimens. An inductive transducer was also used to measure the vertical displacement of the load P point.

3 EXPERIMENTAL RESULTS

3.1 Trajectories of the cracks

Figure 6 shows the crack in a large size TPB specimen with the bed joints at 0° after testing. The crack tried to propagate by the interface brick-mortar, which is the weakness element of the



Figure 6. Crack in a large size TPB specimen with the bed joints at 0° after testing.

specimen. Figure 7 shows the trajectories of the cracks in the TPB large specimens for the 0, 45, 90 and -45 degrees of the bed joint inclination.

Figure 8 shows the cracks in a double-edge notched specimen after testing. The Figure shows the mixed mode cracks and the compression failure cracks in a specimen with vertical bed joints.

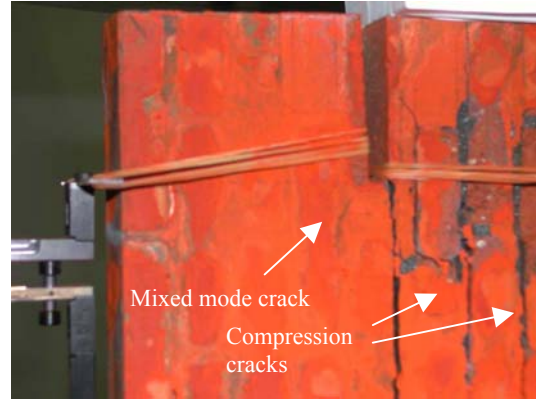


Figure 8. Double-edge crack specimen with vertical bed joints after testing.

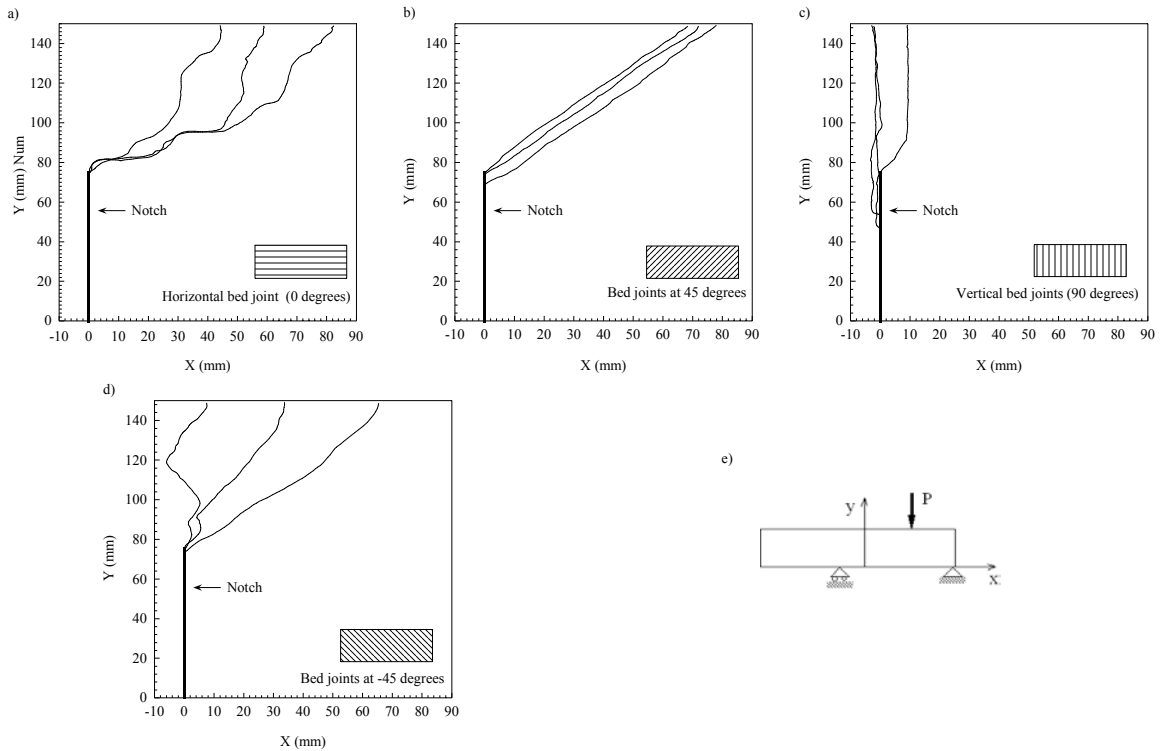


Figure 7. Trajectories of the cracks in the large size TPB specimens ($D = 150$ mm) after testing with the bed joints at: a) 0 degrees, b) 45 degrees, c) 90 degrees, d) -45 degrees, and e) axes of reference.

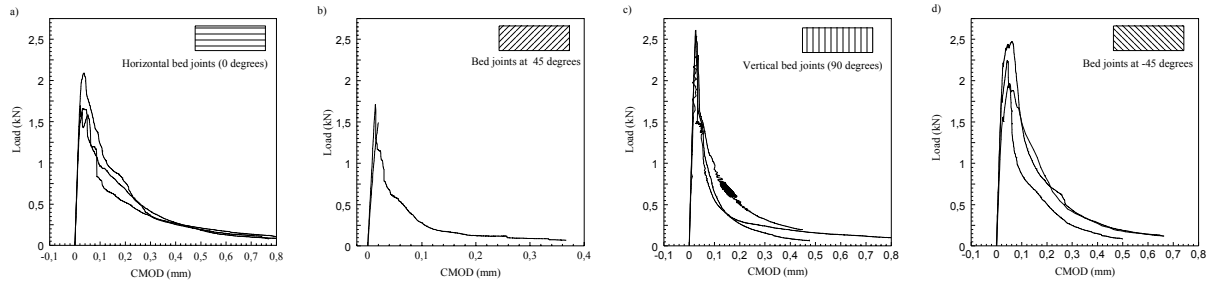


Figure 9. Experimental records for the small size TPB specimens ($D = 75$ mm) of the load P -CMOD with the bed joints at: a) 0 degrees, b) 45 degrees, c) 90 degrees, and d) -45 degrees.

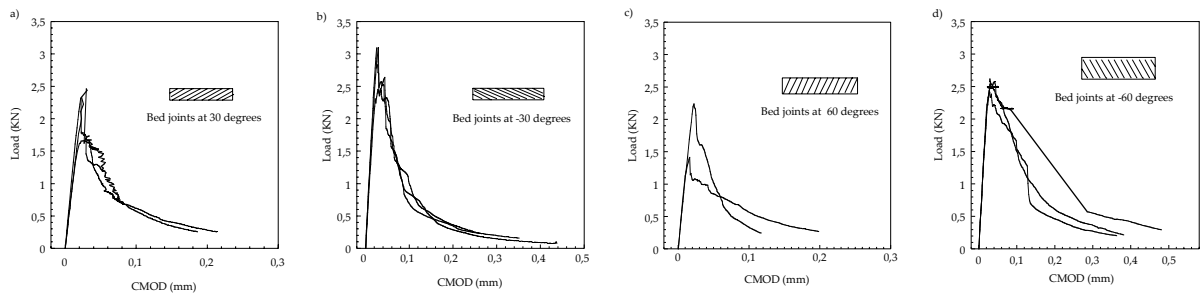


Figure 10. Experimental records for the small size TPB specimens ($D = 75$ mm) of the load P -CMOD with the bed joints at: a) 30 degrees, b) -30 degrees, c) 60 degrees, and d) -60 degrees.

3.2 Load-CMOD curves for TPB specimens

Figures 9 and 10 show the load P versus CMOD experimental curves for the small size ($D=75$ mm) TPB specimens with the bed joints at 0, 45, 90, -45, 30, -30, 60 and -60 degrees. The influence of the bed joints orientation in the peak load is evident. The lowest values were shown by the specimens with the bed joints at 45, 60 and 30 degrees; in these specimens the crack grew by the interface brick-mortar (see Fig. 7a), that is the weakest part of the brickwork masonry. The highest values of the peak load were observed in the specimens with the bed joints at -45, -30 and -60 degrees, where the crack grew crossing brick units and mortar. The curves for the specimens with vertical bed joints (90 degrees) show a high peak load, but cannot be compared with the specimens with other orientations of the bed joints because the crack path is quite different (see Fig. 7c).

3.3 Load-displacement curves for double-edge notched specimens

Figure 11 shows the experimental records load P versus relative displacement of the points situated at height of the tip notches on the lateral vertical faces of the load free part (left extensometer in Fig. 3) of the double-edge notched specimens, for the specimens with the three angles between the load P direction and the bed joints. The curves present a linear first part followed by a curved branch, which return decreasing displacement with the increasing of the load. The return of the curve is caused by the mixed mode crack initiation and propagation from the notch, which reduces the load transmitted by the ligament between the loaded to the load free part of the specimen. The loss of linearity of the curves corresponding to the load free part is not accompanied by an equivalent loss of linearity of the curves corresponding to the loaded part (see Gálvez et al. 2002b). The peak load of the test is governed by the compression failure of the loaded part.

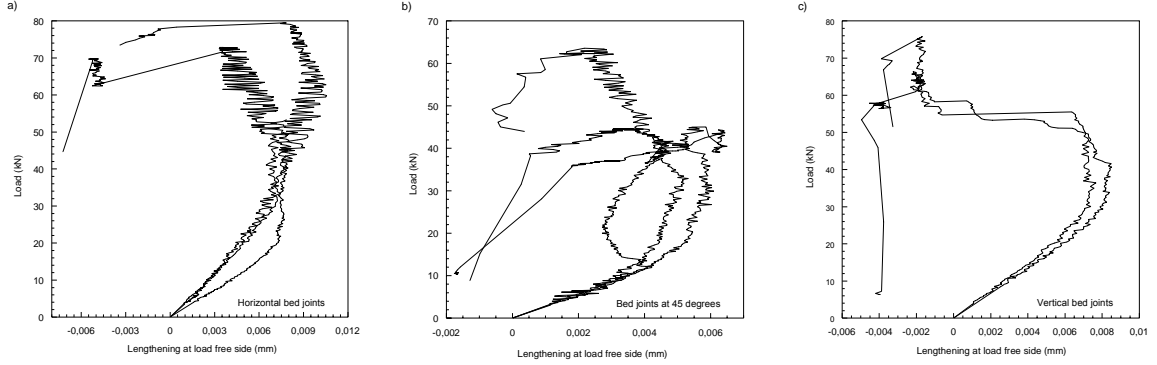


Figure 11. Experimental records for the double-edge notched specimens of the load P -displacement of the load free side of the specimens: a) horizontal bed joints, b) bed joints at 45 degrees, c) vertical bed joints.

4 NUMERICAL MODELLING

4.1 Cracking surface for mixed mode fracture

In this work the discrete crack approach with the cohesive model was adopted (Gálvez et al 2002a).

In mixed mode (I and II) fracture, the relative displacement between the upper and lower faces of the cohesive crack is vectorial in nature. We denote it as \mathbf{u} , with normal and shear components denoted as u_n y u_t , i.e.,

$$\mathbf{u} = u_n \bar{\mathbf{n}} + u_t \bar{\mathbf{t}} \quad (1)$$

where $\bar{\mathbf{n}}$ and $\bar{\mathbf{t}}$ are the unit vectors respectively normal and tangential to the lower crack face.

Likewise, the stress transferred between the faces of the crack is also vectorial, and is characterised by the traction vector \mathbf{t} acting on the lower face of the crack; with the normal and tangential components denoted, respectively, by σ and τ , we have

$$\mathbf{t} = \sigma \bar{\mathbf{n}} + \tau \bar{\mathbf{t}} \quad (2)$$

The formulation of the cohesive crack model in mixed mode thus requires establishing the relationship between the traction vector \mathbf{t} and the crack displacement vector \mathbf{u} . In this study we adopt an elastoplastic formulation in which the crack displacement is split into its elastic and inelastic parts

$$\mathbf{u} = \mathbf{u}^e + \mathbf{u}^i \quad (3)$$

so that the traction vector is given by

$$\mathbf{t} = \mathbf{K}_e \mathbf{u}^e \quad (4)$$

where \mathbf{K}_e is a second order elastic stiffness tensor. In this work we assume that the shear and normal components are uncoupled. We further assume that the normal and shear stiffnesses are identical, so that the matrix of components is actually

$$[\mathbf{K}_e] = K^e \begin{bmatrix} 1 & 0 \\ 0 & 1 \end{bmatrix} \quad (5)$$

Ideally, the initial stiffness of the cohesive crack would have to be infinite to reproduce the rigid-softening behaviour of a cohesive crack. For numerical computations, however, some large but finite value has to be adopted for K^e . In this work we adopted values of K^e so that the normal or shear crack displacement at peak were around $0.001 \omega_c$, where ω_c is the crack displacement for which full softening has occurred.

For the inelastic behaviour, it is assumed that the inelastic crack opening can progress when the so called cracking surface $F(\mathbf{t}) = 0$ is reached, similar to the yield surface in classical plasticity. In this work, the following hyperbolic expression is assumed (Carol et al., 1997):

$$F(\mathbf{t}) = \tau^2 - \tan \phi_f (f_t(\theta) - \sigma) \left[2c(\theta) - \tan \phi_f (f_t(\theta) + \sigma) \right] \quad (6)$$

where $c(\theta)$, ϕ_f and $f_t(\theta)$ are the instantaneous values of the cohesion, friction angle and tensile strength, respectively. These parameters are assumed to depend on the direction of the material, and the loading history only through the effective inelastic crack displacement \mathbf{u}^{ieff} , defined by the conditions

$$\mathbf{u}^{ieff} = \|\dot{\mathbf{u}}^i\| = \left(\dot{u}_n^2 + \dot{u}_t^2 \right)^{0.5} \quad (7)$$

$$u^{ieff} = \int \dot{u}^{ieff} dt \quad (8)$$

In this work we assume that, for a given material, the friction angle ϕ_f is constant, while the instantaneous tensile strength $f_t(\theta)$ and cohesion $c(\theta)$ depend on u^{ieff} bilinearly as depicted in Fig. 12. For an anisotropic material the values of f_{t0} and c_0 depends on the direction of the material. We assume a linear variation from the maximum to the minimum value of f_{t0} and c_0 as a function of the material angle. The area enclosed between the softening curve for f_t and the axes is the specific fracture energy G_F^I for Mode I (usually called fracture energy). The area defined by the softening curve for the cohesion and the axes, has also dimensions of energy per unit area and was called the Mode IIa specific fracture energy G_F^{IIa} by Cervenka (1994). G_F^{IIa} is not accessible to direct measurement in the sense that no test can be devised in which the work of fracture is uniquely related to G_F^{IIa} .

The bilinear softening curve for the tensile strength (Fig. 12a) can be determined experimentally from mode I tests. At present there is no way to directly measure the softening curve for the cohesion. Therefore, we assume that the shape of the two curves is the same and that the effective crack opening at which the strength or cohesion becomes zero is the same. This leads to the following conditions for the characteristic points of the curve:

$$\omega_c = \omega_\sigma, \quad \omega_{1c} = \omega_{1\sigma}, \quad c_0 = f_{t0} \frac{G_F^{IIa}}{G_F^I}, \quad (9)$$

$$s_{1c} = s_{1\sigma} \frac{G_F^{IIa}}{G_F^I}$$

Since, as already pointed out, the characteristic parameters of the softening curve for the instantaneous tensile strength (namely f_{t0} , $s_{1\sigma}$, $w_{1\sigma}$ and w_σ and also the fracture energy G_F^I) are determined from independent mode I tests for each particular material, the complete softening behaviour is fully defined by the mode II fracture energy G_F^{IIa} , or by the ratio G_F^{IIa} / G_F^I .

Figure 13 shows the cracking surface and its evolution in several cracking conditions, based on the value of the parameter u^{ieff} . It is worth noting that the cracking surfaces family depends on the material angle, θ . Note that for each state of damage the cracking surface has two branches and only the branch extending towards negative values of σ is physically acceptable.

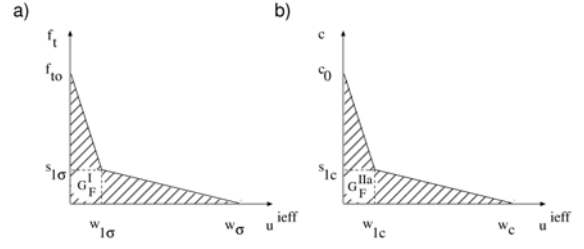


Figure 12. Softening curves for brickwork masonry: a) tensile strength, σ , b) cohesion, c

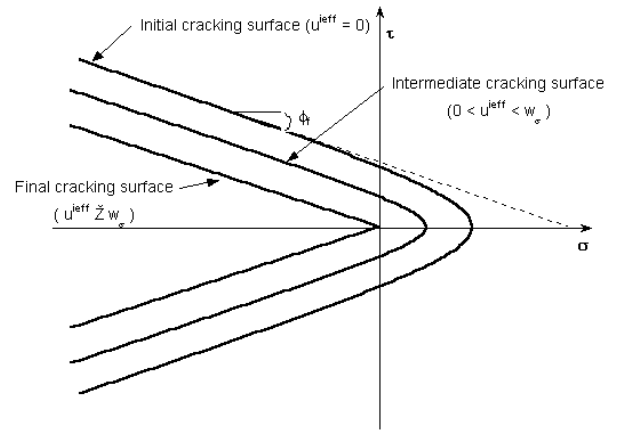


Figure 13. Cracking surface and evolution.

Details about the classical plasticity formulation adopted: flow rule, dilatancy and integration of the rate equations, as well as the numerical implementation in a finite element code may be found in Galvez et al. (2002b).

5 SIMULATION OF THE EXPERIMENTAL TESTS

Figure 14 shows the experimental results and the numerical prediction of the load P -CMOD for the large size TPB specimens ($D = 150$ mm) with different bed joints orientations: horizontal, ± 45 degrees and vertical. The numerical model is a good prediction of the experimental results. Similar results were achieved for the small size TPB specimens.

Figure 15 shows the experimental results and the numerical prediction of the load P versus displacement recorded by the extensometer placed in the load free side of the double-edge specimens (see Fig. 3). The numerical model is also a good prediction of the experimental results.

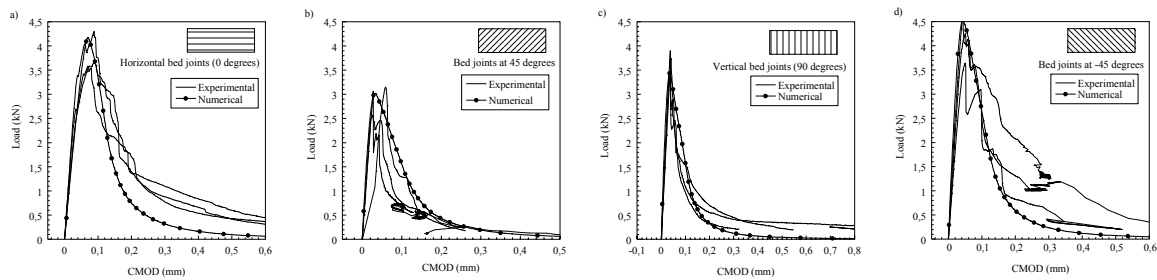


Figure 14. Experimental records and numerical prediction for the large size TPB specimens ($D = 150$ mm) of the load P -CMOD with the bed joints at: a) 0 degrees, b) 45 degrees, c) 90 degrees, and d) -45 degrees.

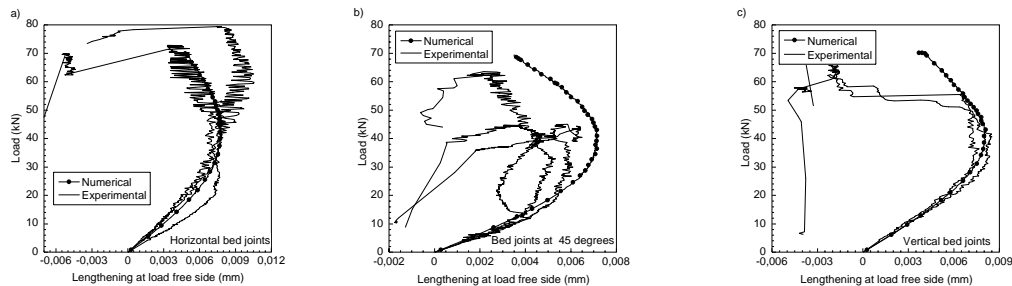


Figure 15. Experimental records and numerical prediction for the double-edge notched specimens of the load P -displacement of the load free side of the specimens: a) horizontal bed joints, b) bed joints at 45 degrees, c) vertical bed joints.

6 FINAL REMARKS

Two testing procedures, for mixed mode fracture of brickwork masonry, were presented. These procedures were successful for other quasi brittle materials. They were applied to study the mixed mode failure of the brickwork masonry with different bed joints orientations and two similar sizes of specimens. The experimental results showed a narrow scatter band and may be used as bench mark for analytical and numerical models for masonry fracture.

A numerical model was also proposed. The model is based on the cohesive approach and takes into account the anisotropy of the masonry. The model has been implemented in a finite element code and properly predicts the experimental results.

ACKNOWLEDGEMENTS

The authors gratefully acknowledge the financial support for this research provided by the Spanish Ministerio de Educación y Cultura under grant MAT2001-3863-CO3-02 and by the European Community under grant EVK4-2001-00091.

Also complementary financial support by Junta de Comunidades de Castilla La Mancha under grant PBI-02-006 is acknowledged.

REFERENCES

- American Concrete Institute 1999a. ACI 530-99. *Building Code Requirements for Masonry Structures*. Detroit: ACI.
- American Concrete Institute 1999b. ACI 530.1-99. *Specification for Masonry Structures*. Detroit: A.C.I.
- Bosiljkov, V., Zarnic, R., Kralj, B. & Pande, G.N. 1998. Experimentally-based computational modelling of masonry. In *Computer Methods in Structural Masonry-4*. New York: E&FN Spon: 103-110.
- Carol, I., Prat, P. & López, M. 1997. Normal/shear cracking model: application to discrete crack analysis. *J. of Eng. Mechanics ASCE* 123(8): 765-773.
- Gálvez, J.C., Elices, M. & Cendón, D.A. 1999. Fracture of double-edge notched specimens under compression loading. In *Construction Materials: Theory and Application*. Stuttgart: Ibidem-Verlag: 95-105.
- Gálvez, J.C., Cervenka, J., Saouma, V. & Cendón, D.A. 2002a. A discrete crack approach to normal/shear cracking of concrete. *Cement and Concrete Res.* 32: 1567-1585.
- Gálvez, J.C., Reyes, E. & Casati, M.J. 2002b. Brick masonry failure under tensile/shear loading. In *6th International Masonry Conference*. London: 184-191.
- Jukes, P. & Riddintong, J.R. 2001. The failure of brick triplet test specimens. *Masonry International* 15(1): 30-33.
- Lorenço, P.J. 1996. *Computational strategies for masonry structures*, Ph.D. Thesis Delft University of Technology.
- Lorenço, P.J., Rots, J. & Blaauwendraad, J. 1996. Continuum model for masonry parameter estimation and validation. *J. of Struct. Eng. ASCE* 124(6): 642-652.